

Low-Dimensional Photocatalysts for CO₂ Conversion

Subjects: Materials Science, Characterization & Testing

Contributor: Hyeonseok Lee

The ongoing energy crisis and global warming caused by the massive usage of fossil fuels and emission of CO₂ into atmosphere continue to motivate researchers to investigate possible solutions. The conversion of CO₂ into value-added solar fuels by photocatalysts has been suggested as an intriguing solution to simultaneously mitigate global warming and provide a source of energy in an environmentally friendly manner. There has been considerable effort for nearly four decades investigating the performance of CO₂ conversion by photocatalysts, much of which has focused on structure or materials modification. In particular, the application of low-dimensional structures for photocatalysts is a promising pathway. Depending on the materials and fabrication methods, low-dimensional nanomaterials can be formed in zero dimensional structures such as quantum dots, one-dimensional structures such as nanowires, nanotubes, nanobelts, and nanorods, and two-dimensional structures such as nanosheets and thin films. These nanostructures increase the effective surface area and possess unique electrical and optical properties, including the quantum confinement effect in semiconductors or the localized surface plasmon resonance effect in noble metals at the nanoscale.

Keywords: photocatalysis ; carbon dioxide conversion ; nanostructures ; low-dimensional photocatalysts ; solar fuels

1. Background

The fast-developing modern technology and explosive world population growth have resulted in a huge demand for and consumption of energy. According to an investigation from the U.S. Energy Information Administration, more than 600 quadrillion Btus of energy were spent in 2020 and it is expected that the demand will continue to skyrocket annually. To meet this huge energy demand every year, energy production has been predominately dependent on fossil fuels such as coal, oil, or natural gas. The energy production by fossil fuels is inextricably linked to the gigantic CO₂ emission of more than 30 billion metric tons every year and, in turn, the accumulated CO₂ in our atmosphere is deemed to be the main cause of many environmental problems such as global warming and erratic weather patterns. In this context, there is great motivation to find a way of reducing atmospheric CO₂ and producing energy at the same time. For these problems, CO₂ conversion by photocatalyst materials under light illumination could be an expedient solution. This is because natural sunlight provides clean, renewable, and abundant energy, and photocatalysts can be activated by light energy from the Sun, while simultaneously consuming CO₂ for energy production.

In 1978, by Halmann ^[1], the first demonstration of the photocatalytic conversion of CO₂ in aqueous solution into liquid fuels such as methanol, formic acid, and formaldehyde was achieved over p-type gallium phosphide semiconductor. The same year, the photoartificial synthesis by SrTiO₃ photocatalysts for CH₄ production through the gas-solid phase reaction of CO₂ and H₂O was reported by Hemminger ^[2]. In 1979, another pioneering work by Fujishima and his coworkers introduced the artificial synthesis of solar fuels from a CO₂-saturated electrolyte under light illumination. In this study, liquid CO₂ was converted with various semiconductor photocatalysts such as TiO₂, ZnO, CdS, GaP, SiC, and WO₃ to produce methane, methanol, formaldehyde and formic acid ^[3]. Since these historical works mentioned above, several semiconductor materials have been investigated for the conversion of CO₂ into useful fuels, including graphitic carbon nitride (g-C₃N₄), graphene, conjugated polymers, covalent organic framework, metal organic frameworks, metal chalcogenides, metal oxides, black phosphorus, bismuth-based materials, and perovskites ^{[4][5][6][7][8][9][10][11][12][13][14]}. Moreover, a variety of strategies and approaches have been applied to improve the photocatalyst performance through elemental doping, solid solution, heterostructure, nanostructuralization, surface engineering and modification, crystal facet engineering, cocatalysts utilization, or dimensionality tailoring ^{[15][16][17][18][19]}.

Of the strategies researched to boost the efficiency of CO₂ conversion, decreasing the dimensionality and constructing nanostructures of the photocatalyst have attracted a lot of attention owing to their favorable advantages in photocatalysis: first, nanostructured photocatalysts suppress the carrier recombination due to their higher crystallinity compared to non-nanostructured materials ^{[20][21][22]}; second, the implementation of low dimensionality modifies the electronic structure of bulk materials due to the quantum confinement effect in semiconductors or localized surface plasmon resonance effect in

noble metals at the nanoscale; third, low-dimensional materials possess larger surface-area-to-volume ratio in comparison with bulk materials, providing more reaction sites. All three features can contribute to improved solar-driven catalytic reactions [19][23].

2. The Main Fundamentals of CO₂ Photoconversion into Solar Fuels and Hydrocarbon Species

2.1. Nature of CO₂

Carbon dioxide (CO₂) is one of the primary greenhouse gases but, at the same time, it is the main resource for solar fuel production when coupled with proton donors such as H₂O for photocatalytic CO₂ conversion. Hence, understanding the nature of the gaseous CO₂ molecule itself is necessary for efficient utilization of photocatalysts. CO₂ is a stable linear molecule among carbon compounds because of it is in the highest oxidation state of carbon, C⁺⁴ [19]. The CO₂ molecule has two C=O bonds with a dissociation energy of ~750 kJ/mol, which is quite larger than those in other chemical bonds such as C-H (~430 kJ/mol) and C-C (~336 kJ/mol). For this reason, the reduction of CO₂ to produce solar fuels requires additional energy to break the C=O bond and form, for example, a C-H bond [24]. Owing to its stability and strong bonding, photocatalytic reduction of CO₂ into solar fuels can be achieved primarily with the support of proton donors such as H₂O or H₂ [25].

2.2. CO₂ Adsorption on the Surface of Photocatalysts

The adsorption and activation of CO₂ on a solid surface is one of the essential steps in achieving CO₂ reduction and photocatalytic performance. The adsorption mechanism of CO₂ on several semiconductor photocatalysts has been investigated [26][27]. For instance, the adsorption of CO₂ on TiO₂ surface has been investigated by Minot and coworkers [26]. Various adsorption modes of CO₂ over a rutile TiO₂ surface have been studied using first-principles calculations. The oxygen atom of CO₂ molecules favors the interaction with the acidic titanium cation over the surface forming a Ti-OCO bond [26]. The adsorption of CO₂ on a photocatalyst surface includes the interaction between the CO₂ molecule and the surface atoms of the photocatalyst. This absorption may occur with a charge transfer from the photocatalyst to the linear and stable CO₂ molecule which can induce the formation of partially charged and bent adsorbate, CO_{δ-2}, and this adsorbate can form three different molecular structures, as shown in Figure 1: oxygen coordination, carbon coordination, and mixed coordination [24][28][29]. The beneficial feature of CO_{δ-2}, is that it has decrease in the lowest unoccupied molecular orbital (LUMO) of the CO₂ energy level as linear CO₂ molecule transformed into the bent structure. This would facilitate the charge transfer between a photocatalyst and CO_{δ-2}, [24][28][29].

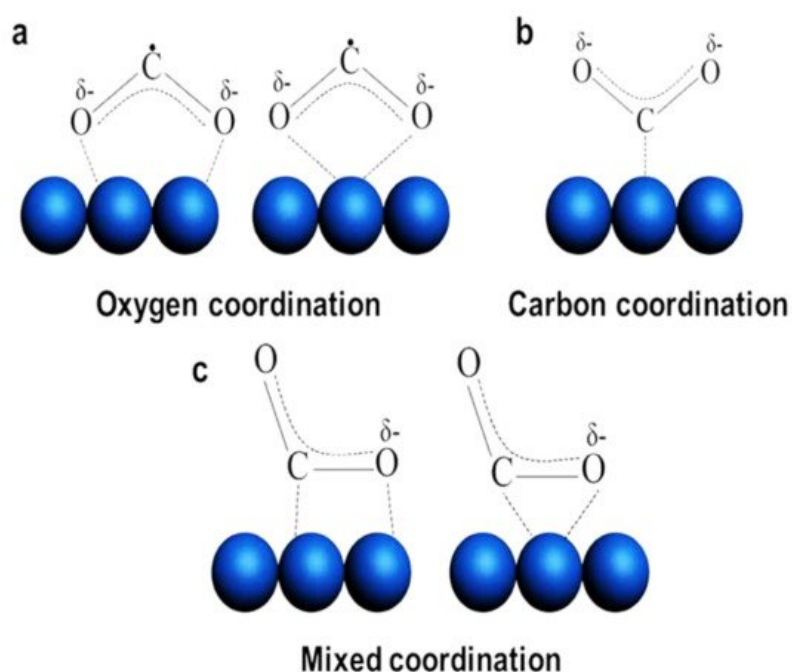


Figure 1. Schematic illustration of the different types of CO₂ adsorption modes (Adapted from [24]).

In the photocatalytic reaction, the photocatalyst donates electron to the adsorbed species on the surface to initiate the reduction process of CO₂ in the presence of protons. As shown in Table 1, the solar fuel production is determined by the number of electrons and protons included in the reaction [20][24]. For example, two electrons are required for CO evolution, while methane production is an eight-electron reaction. The adsorption of CO₂ on the photocatalyst surface can be

improved by a variety of strategies. First, decreasing the structural dimensionality of photocatalyst can improve the surface area of the photocatalyst to allow more adsorption. Second, enhanced density of active sites by incorporation of surface defects, such as oxygen and sulfur vacancies, can improve the CO₂ adsorption. Third, utilization of noble metal nanoparticles can help improve the adsorption due to lowered activation energy of the CO₂ reduction [24][30].

Table 1. Standard electrochemical potentials of CO₂ and H₂O at 25 °C and atmospheric pressure [20][24].

Reaction	E° at pH 7 (V vs. NHE)	Solar Fuel
CO ₂ reduction	$\text{CO}_2 + 2\text{H}^+ + 2\text{e}^- \rightarrow \text{CO} + \text{H}_2\text{O}$	-0.51 CO
	$\text{CO}_2 + 8\text{H}^+ + 8\text{e}^- \rightarrow \text{CH}_4 + 2\text{H}_2\text{O}$	-0.24 CH ₄
	$\text{CO}_2 + 6\text{H}^+ + 6\text{e}^- \rightarrow \text{CH}_3\text{OH} + \text{H}_2\text{O}$	-0.39 CH ₃ OH
	$2\text{CO}_2 + 12\text{H}^+ + 12\text{e}^- \rightarrow \text{C}_2\text{H}_5\text{OH} + 3\text{H}_2\text{O}$	-0.33 C ₂ H ₅ OH
	$\text{CO}_2 + 2\text{H}^+ + 2\text{e}^- \rightarrow \text{HCOOH}$	-0.58 HCOOH
	$\text{CO}_2 + 4\text{H}^+ + 4\text{e}^- \rightarrow \text{HCHO} + \text{H}_2\text{O}$	-0.48 HCHO
H ₂ O oxidation	$2\text{H}_2\text{O} \rightarrow \text{O}_2 + 4\text{H}^+$	+0.81 O ₂

2.3. The Mechanism of Efficient CO₂ Photoconversion

Upon absorption of light over the photocatalyst, charge carrier pairs are generated to achieve the photosynthesis of solar fuels accompanying the water splitting as shown in Table 1. To execute the conversion of CO₂ into useful fuels from the thermodynamic point of view, the conduction band minimum (CBM), and the valence band maximum (VBM) of a photocatalyst should bracket the redox potential of CO₂ and the oxidation potential of water, respectively, as shown in Table 1 and Figure 2. As results of the reactions, various solar fuels can be formed dependent on the number of electrons and protons in the presence of CO₂ and water under the illumination.

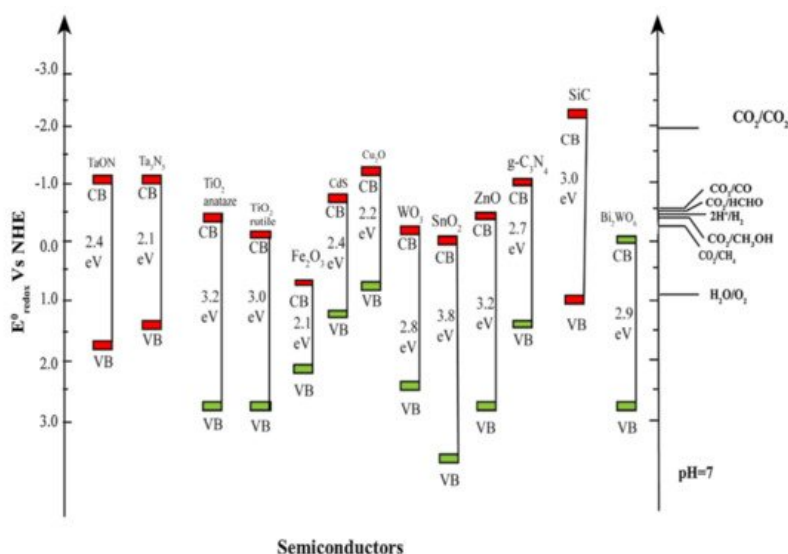


Figure 2. The energy band structures of semiconductor photocatalysts and the corresponding redox potentials of CO₂ reduction into solar fuels (Adapted from [31]).

The artificial photosynthesis of solar fuels using semiconductor photocatalysts consists of three essential steps, as described in Figure 3. Firstly, incident photons of light with energy higher than that of semiconductor band gap (E_g) induce the generation of the electron-hole pairs (Process (i)). Secondly, the photogenerated charge carriers are transferred to the photocatalyst surface (Process (ii)). Thirdly, the electrons and holes react on the surface of photocatalyst with CO₂ and H₂O for evolution of solar fuels (Process (iii)). For efficient photocatalytic conversion of CO₂ into fuels, the ideal semiconductor photocatalyst should have optimized band gap for efficient light harvesting and photocarrier generation, facile charge separation and transportation, vigorously activated sites and high surface area for maximum adsorption of CO₂ and water [30][32].

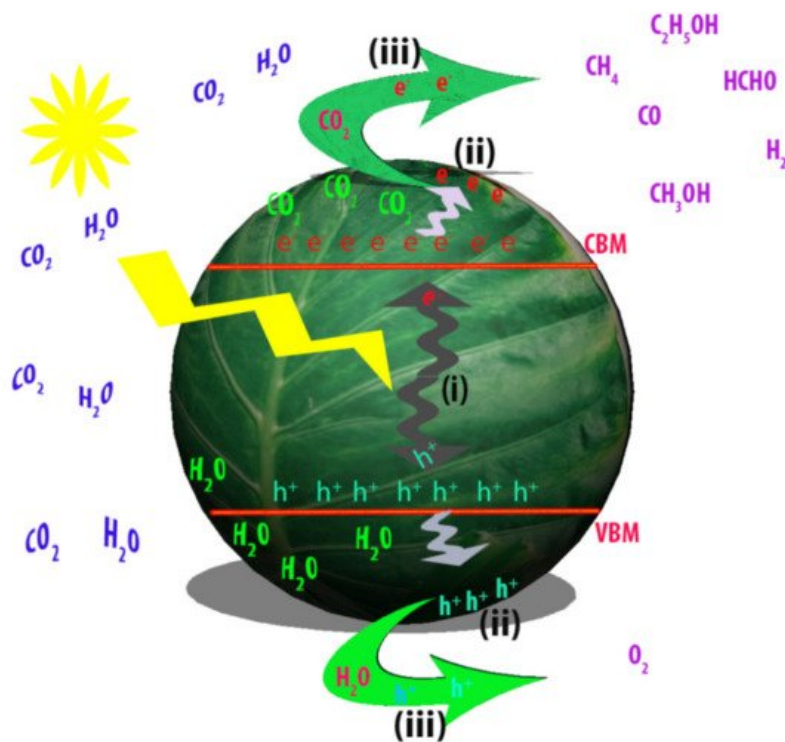


Figure 3. A schematic diagram of CO₂ photocatalytic conversion process over photocatalyst. Process (i): light absorption and generation of photocarriers via a semiconductor photocatalyst. Process (ii): charge carrier separation and transfer to the surface of photocatalyst. Process (iii): reactions of CO₂ and H₂O with electrons and holes, respectively to produce solar fuels.

3. Strategies for Enhancement in the Light-Driven CO₂ Conversion over Low-Dimensional Photocatalysts

Applying low-dimensional structure to the photocatalytic system itself is a proven way for obtaining high CO₂ conversion performance. However, further improvement is available by designing the structures or modifying the photocatalytic materials so that characteristics of photocatalysts or photocatalytic system are engineered. Here, we focus on these two major strategies for further enhancement of CO₂ conversion by low-dimensional photocatalysts. [Table 2](#) summarizes the examples mentioned in this section.

Table 2. Summary of low-dimensional photocatalysts used in photocatalytic reduction of CO₂ into solar fuels. NC: Nanocrystal, GQD: Graphene Quantum Dot, NF: Nanofiber, NS: Nanosheet, CNT: carbon nanotube, Mt: montmorillonite, m-CN: modified g-C₃N₄, NR: nanorod, NW: nanowire, CND: carbon nano dot, p-CN: protonated g-C₃N₄, PGCN: porous g-C₃N₄, TEOA: triethanolamine, bpy: bipyridine, C₃N₄: Melon-based polymeric carbon nitride, UTNS: ultrathin nanosheet, P-g-C₃N₄: Phosphorus doped g-C₃N₄.

Dimensionality	Morphology	Photocatalyst	Light Source	Reducing Agent	Main Product	Activity [$\mu\text{mol}\cdot\text{g}^{-1}\cdot\text{h}^{-1}$]	Ref.
0D	QD 3–12 nm	CsPbBr ₃	300 W Xe lamp	H ₂ O	CO CH ₄	4.26 1.53	[33]
	QD 2.3 nm	Cs ₃ Bi ₂ I ₉	300 W Xe lamp	H ₂ O	CO	1.15	
	QD 2.9 nm	Cs ₃ Bi ₂ Br ₉	300 W Xe lamp	H ₂ O	CO	26.95	[34]
	QD 2.4 nm	Cs ₃ Bi ₂ Cl ₉	300 W Xe lamp	H ₂ O	CO	21.01	
	NC 9.5 nm	Cs ₂ AgBiBr ₆	AM 1.5G	Ethyl acetate	CO CH ₄	2.35 1.6	[35]
	QD 9.45 nm	FAPbBr ₃	300 W Xe arc lamp	H ₂ O	CO CH ₄	181.25 16.9	[36]
	QD 5.86 nm	GQD	300 W Xe lamp 420 nm cutoff filter	H ₂ O	CH ₃ OH	0.695	[11]
	NR	CeO ₂	300 W Xe lamp	H ₂ O	CO	0.020	[37]
1D	NT	TiO ₂	300 W Xe arc lamp 320 nm < λ < 780 nm	H ₂ O	CH ₄	2.128	[21]
	NR	TiO ₂	300 W Xe arc lamp 320 nm < λ < 780 nm	H ₂ O	CH ₄	1.41	[21]
	NT	P-g-C ₃ N ₄	300 W Xe lamp	H ₂ O/TEOA	CO CH ₄	2.37 1.81	[38]
	NT	PGCN	300 W Xe lamp	H ₂ O/MeCN/TEOA	CO	103.6	[39]
	NT	Bi ₁₂ O ₁₇ Cl ₂	300 W Xe lamp	H ₂ O	CO	48.6	[40]
	NT	Bi ₁₂ O ₁₇ Br ₂	300 W Xe lamp	H ₂ O	CO	34.5	[41]
	NS	g-C ₃ N ₄	300 W Xe arc lamp	MeCN/TEOA (4:1)	CO CH ₄	5.407 1.549	[42]
	UTNS	g-C ₃ N ₄	300 W Xe lamp	H ₂ O	CH ₄ CH ₃ OH	1.39 1.87	[43]
2D	UTNS	SiC	300 W Xe lamp	H ₂ O	CO CH ₄	1.29 3.11	[44]
	UTNS	Bi ₂ MoO ₆	300 W Xe lamp	H ₂ O	CO	3.62	[45]
	QD/NW	Black P/WO ₃	300 W Xenon arc lamp	H ₂ O	CO C ₂ H ₄	~ 135 ~ 11	[13]
	QD (10 nm)/NT	WS ₂ /Bi ₂ S ₃	300 W Xe arc lamp	H ₂ O	CH ₃ OH C ₂ H ₅ OH	9.55 6.95	[46]
	QD (3.5 nm)/NW	Ti ₃ C ₂ /Cu ₂ O	300 W Xe lamp	H ₂ O	CH ₃ OH	78.50	[47]

Dimensionality	Morphology	Photocatalyst	Light Source	Reducing Agent	Main Product	Activity [$\mu\text{mol}\cdot\text{g}^{-1}\cdot\text{h}^{-1}$]	Ref.
0D/2D	QD (1.6 nm)/NS	CuO/WO ₃	300 W Xe lamp $\lambda > 400$ nm	H ₂ O	CO	1.58	[48]
	ND (4.4 nm)/NS	CND/p-CN	Xe arc lamp	H ₂ O	CO CH ₄	5.88 2.92	[49]
	QD/NS	TiO ₂ /g-C ₃ N ₄	300 W Xe lamp $\lambda > 400$ nm	MeCN/TEOA	CO	77.8	[50]
	QD (5nm)/NS	Au/TiO ₂	300 W Xe arc lamp	H ₂ O	CO CH ₄	19.75 70.34	[51]
	QD (7nm) /NS	CsPbBr ₃ /Bi ₂ WO ₆	300 W Xe lamp $\lambda > 400$ nm	H ₂ O	CO/CH ₄	503 $\mu\text{mol}\cdot\text{g}^{-1}$	[52]
1D/2D	NF/NS	TiO ₂ /MoS ₂	350 W Xe lamp	H ₂ O	CH ₄ CH ₃ OH	2.86 2.55	[53]
	NT/NS	CNT/g-C ₃ N ₄	200 W Hg and solar simulator	H ₂ O	CO CH ₄	410 74	[54]
	NR/NS/NF	Au/TiO ₂ /BiVO ₄	300 W Xe lamp	H ₂ O	CO CH ₄	2.5 7.5	[55]
	NS/NS	Ti ₃ C ₂ /Bi ₂ WO ₆	300 W Xe lamp	H ₂ O	CH ₄ CH ₃ OH	1.78 0.44	[56]
	NS/NS	Bi ₂ WO ₆ /BiOI	500 W Xe arc lamp $\lambda < 400$ nm	H ₂ O	CH ₄	2.92	[57]
2D/2D	NS/NS	Mt/m-CN	35 W Xenon lamp	H ₂ O/H ₂	CO CH ₄	505 330	[58]
	NS/NS	SnS ₂ /TiO ₂	300 W Xe lamp	H ₂ O	CH ₄	23	[59]
	NS/NS	g-C ₃ N ₄ /BiVO ₄	300 W Xe lamp $\lambda \geq 420$ nm	H ₂ O	CO CH ₄	5.19 4.57	[60]
	NS/NS	PGCN/Bi ₁₂ O ₁₇ Cl ₂	300 W xenon lamp	H ₂ O	CH ₄	24.4	[61]
	NP-NS/NS	Pd-g-C ₃ N ₄ /RGOA	300 W Xe lamp	H ₂ O	CH ₄	6.4	[62]

3.1. Construction of Junction Formed by Low-Dimensional Structures

Of the diverse strategies to promote CO₂ conversion performance of photocatalysts, designing or formation of junctions in photocatalytic systems has seen some success by modifying optical and electrical properties through materials and interfaces [51]. Junctions are constructed by coupling of two or more semiconductor materials or metal materials. The formation of a junction allows valuable properties from various materials to be more available in a single system. That helps more efficient light absorption, charge separation and transfer, or more stable performance. Since the photocatalytic systems with junctions have single or multiple interfaces, the engineering of the interfacial characteristics between the materials is essential for efficient photocatalyst performance. Especially, the interface characteristics can influence on carrier behaviors through bulk or at interfaces (ex. Shockley-Read-Hall recombination).

The formation of junctions implies the presence of an internal electric field in the nanomaterial. This internal electric field can contribute to enhanced carrier behaviors such as carrier separation and transfer for the photo-induced charge carriers and to, in the end, the performance of light-driven CO₂ conversion. The internal electric field can be induced by growth of a low-dimensional semiconductor on a low-dimensional semiconductor [23][63]. The combination of two or multiple low-dimensional materials could integrate the advantages of both single units and mitigate the shortcomings of single unit by the synergistic effect [64].

One of the advantages of semiconductor QDs is the quantum size effect which is responsible for the optical properties of the photocatalyst. Apart from the acceleration of charge separation and transfer process, the contact between 0D semiconductor and 1D semiconductor provides the nanocomposite with an additional properties such as excessive electroactive sites, high surface area, and homogenous dispersion [65]. 1D Bi₂S₃ nanotubes have outstanding ability to absorb visible and near infrared light. The tubular structure of Bi₂S₃ provides the photocatalytic reaction with more active

sites than other morphologies [46]. The remarkable optical and electronic properties of tungsten disulfide (WS₂) QDs can be realized due to the quantum confinement effect. WS₂ QDs can be also dispersed uniformly on the surface of Bi₂S₃ forming Bi–S channels to facilitate the charge carrier separation transfer process. The designed 0D/1D nanocomposite exhibited outstanding photocatalytic reduction of CO₂ into CH₃OH and C₂H₅OH of 38.2 μmol·g⁻¹ and 27.8 μmol·g⁻¹ after 4 h radiation, respectively. The improved photoreduction performance is related to the following features. Firstly, the 0D/1D nanocomposite provided combined optical and electrical properties of both WS₂ QDs and Bi₂S₃ nanotubes causing high visible and near infrared light absorption. Secondly, the enlarged surface area of the nanocomposite provided more active adsorptions site for CO₂. Thirdly, the low resistive QDs–NTs interface due to the Bi–S bonds plays a critical role for accelerated charge carrier separation [46]. CsPbBr₃ is widely used in the photocatalytic reactions but it suffers from the high rate of recombination during the interface transfer due to the strong reductive ability of electrons [52]. Hence, the suppression of undesired electron loss throughout the transfer process at the interface is critical factor for efficient utilization of CsPbBr₃. Li et al. fabricated 0D/2D nanocomposite of CsPbBr₃/Bi₂WO₆ via ultrasonic method with intimate contact at the interface to improve the charge separation and transfer. The Bi–Br bonds which is formed at the QDs–NSs interface is responsible for the strong interfacial interaction. The decoration of Bi₂WO₆ with CsPbBr₃ QDs could enhance the CO and CH₄ yield by factor of 9.5 over that of pristine CsPbBr₃ [52].

The building of 1D semiconductor materials on 2D semiconductors is an efficient strategy for efficient CO₂ conversion. Coupling of TiO₂ nanofibers with light harvesting semiconductors such as MoS₂ nanosheets is an efficient way to overcome the fast recombination of charge carriers and enhance the light absorption efficiency [53]. The electronic properties of MoS₂ nanosheets can be tuned by control of the thickness. The superior conversion activity of CO₂ into hydrocarbon species, that is, CH₄ and CH₃OH, resulted from the improved light harvesting, sufficient reactive sites for CO₂ adsorption, and the intimate 1D–2D chemical contact between MoS₂ and TiO₂ which could be favorable for facile and efficient charge separation upon photoexcitation [53]. The increase of the contact area between the two semiconductor nanomaterials is much more favorable to enhance the photocatalytic performance over the photocatalyst. In other words, constructing the 2D/2D interface is favorable for highly separated charge carriers at the interface. Wang et al. prepared 2D/2D heterojunctions by growth of ultrathin tin disulfide (SnS₂) onto TiO₂ nanosheets via a hydrothermal method [59]. The production yield of CH₄ over SnS₂/TiO₂ was much higher than that of pristine SnS₂ and TiO₂ nanosheets. The reason for such outstanding performance originates from the increment of the contract area between SnS₂ and TiO₂ nanosheets [59].

The photocatalytic systems with multiple junctions, that is, with multiple interfaces, displays excellent photocatalytic activity toward solar fuels generation compared to one with/without single junction [55][66][67]. Recently, Macyk and coworkers designed two heterointerface-based photocatalyst, TiO₂/C₃N₄/Ti₃C₂, via the interfacial assembly of Ti₃C₂ QDs on the TiO₂/C₃N₄ binary nanocomposite to boost the charge separation and transfer and providing strong redox ability in CO₂ photoreduction reaction [67]. The as-synthesized composite exhibited enhanced light absorption, suppressed electron-hole recombination, and demonstrated stable photocurrent sensitivity. The fabricated composite could overcome the disadvantage of TiO₂/C₃N₄ nanocomposites with a single junction by providing more efficient transport channels of electrons-hole pairs due to the strong interaction between Ti₃C₂ QDs and TiO₂/C₃N₄ NS. Theoretical studies demonstrated that construction of two interfacial electric fields between TiO₂/C₃N₄ and Ti₃C₂/C₃N₄ is due to electron transfer processes at the two interfaces. The interfacial built-in electric fields can promote the charge carrier separation and the photocatalytic reduction of CO₂ into CO and CH₄. Tonda et al. fabricated another multijunction system with a Bi₂WO₃/RGO/g-C₃N₄ 2D/2D/2D architecture using two-step hydrothermal method for utilization in CO₂ and water reduction into useful fuels [66]. This ternary heterojunction exhibited highly improved characteristics in light harvesting ability, CO₂ adsorption capacity, photocurrent responses, and interfacial contact area. The photoconversion performance of CO₂ over Bi₂WO₃/RGO/g-C₃N₄ was dramatically enhanced toward CH₄ and CO evolution. The performance of Bi₂WO₃/RGO/g-C₃N₄ was 2.5 times higher and 3.8 times higher than those of Bi₂WO₃/RGO and RGO/g-C₃N₄, respectively [66].

3.2. Modification of Low-Dimensional Nanomaterials

Modification of nanostructured low-dimensional photocatalysts themselves are another beneficial strategy for the enhancement of photocatalytic CO₂ conversion because it helps the properties of photocatalysts to be engineered. The modification can be achieved using several approaches such as introduction of surface oxygen vacancies or the formation of a porous structure.

The efficient utilization of the solar spectrum can be controlled by tuning the band structure of the semiconductor using the elemental doping [19]. Yu et al. synthesized oxygen-doped g-C₃N₄ nanotubes via exfoliation and a 3D g-C₃N₄ curling condensation method [68]. It was found that the synthesized photocatalyst consisted of curled nanosheets that had a uniform tubular structure with 20–30 nm of diameter. The oxygen atoms can substitute for the C or N atoms in g-C₃N₄ under high temperature oxidation conditions. The oxygen doping of 1D g-C₃N₄ helped the conduction band to be at

a more positive potential causing a narrower band gap and efficient light harvesting. This structure exhibited a significant methanol evolution rate of $0.88 \mu\text{mol}\cdot\text{g}^{-1}\cdot\text{h}^{-1}$ under visible light radiation. Wu et al. synthesized self-doped black TiO_2 nanotubes arrays using a one-step aluminothermic reduction for solar-driven conversion of CO_2 into CO [69]. It is found that the average diameter of the nanotubes was 75–85 nm with 5–7 nm of wall thickness. The oxygen vacancies can act as active sites for CO_2 molecules for efficient photogenerated charge carrier separation. The visible light absorption of black TiO_2 was largely enhanced by virtue of the oxygen vacancies. The resulted photocatalytic conversion was $185.39 \mu\text{mol}\cdot\text{g}^{-1}\cdot\text{h}^{-1}$ of CO evolution rate under visible light.

The introduction of defects into semiconductors can improve the photocatalytic activity of CO_2 into solar fuels ascribed to the promotion of photogenerated charge carrier separation and the extended light absorption [70]. Liu and coworkers prepared $\text{Bi}_{12}\text{O}_{17}\text{Cl}_2$ nanotubes with surface oxygen defects via solvothermal method [40]. The tubular structure plays crucial role for accelerating the photogenerated charge carrier separation, while the oxygen defects on the surface act as active centers for CO_2 activation. It is found that the absorption of $\text{Bi}_{12}\text{O}_{17}\text{Cl}_2$ nanotubes is improved in the visible region compared to its bulk counterpart. The defective ultrathin tubular structure of $\text{Bi}_{12}\text{O}_{17}\text{Cl}_2$ provides effective CO_2 conversion into CO with production yield of 16.8 times higher than bulk $\text{Bi}_{12}\text{O}_{17}\text{Cl}_2$. The higher photocatalytic conversion rate can be attributed to faster charge separation on the surface of $\text{Bi}_{12}\text{O}_{17}\text{Cl}_2$ nanotubes.

The porosity of nanostructured semiconductors provides an additional feature to increase the surface area of photocatalysts, and subsequently is favorable for the solar-driven reduction of CO_2 into valuable fuels [71]. Huang et al. used a template-free method to prepare porous g- C_3N_4 with increased surface area [72]. It is reported that the porous g- C_3N_4 nanotubes had excellent photocatalytic conversion of CO_2 into CO of $40 \mu\text{mol}\cdot\text{g}^{-1}$ within 4 h illumination. The CO yield was higher than that of bulk g- C_3N_4 by a factor of 5.6 originated from the higher surface area of the porous tubular structure, and the improved charge carrier separation and transfer process.

References

1. Halmann, M. Photoelectrochemical reduction of aqueous carbon dioxide on p-type gallium phosphide in liquid junction solar cells. *Nature* 1978, 275, 115–116.
2. Hemminger, J.; Carr, R.; Somorjai, G. The photoassisted reaction of gaseous water and carbon dioxide adsorbed on the SrTiO_3 (111) crystal face to form methane. *Chem. Phys. Lett.* 1978, 57, 100–104.
3. Inoue, T.; Fujishima, A.; Konishi, S.; Honda, K. Photoelectrocatalytic reduction of carbon dioxide in aqueous suspensions of semiconductor powders. *Nature* 1979, 277, 637–638.
4. Zeng, S.; Kar, P.; Thakur, U.K.; Shankar, K. A review on photocatalytic CO_2 reduction using perovskite oxide nanomaterials. *Nanotechnology* 2018, 29, 052001.
5. Zhou, B.; Song, J.; Xie, C.; Chen, C.; Qian, Q.; Han, B. Mo–Bi–Cd Ternary Metal Chalcogenides: Highly Efficient Photocatalyst for CO_2 Reduction to Formic Acid Under Visible Light. *ACS Sustain. Chem. Eng.* 2018, 6, 5754–5759.
6. Bie, C.; Zhu, B.; Xu, F.; Zhang, L.; Yu, J. In situ grown monolayer N-doped graphene on CdS hollow spheres with seamless contact for photocatalytic CO_2 reduction. *Adv. Mater.* 2019, 31, 1902868.
7. Billo, T.; Shown, I.; Kumar Anbalagan, A.; Effendi, T.A.; Sabbah, A.; Fu, F.-Y.; Chu, C.-M.; Woon, W.-Y.; Chen, R.-S.; Lee, C.-H. A mechanistic study of molecular CO_2 interaction and adsorption on carbon implanted SnS_2 thin film for photocatalytic CO_2 reduction activity. *Nano Energy* 2020, 72, 104717.
8. Li, D.; Kassymova, M.; Cai, X.; Zang, S.-Q.; Jiang, H.-L. Photocatalytic CO_2 reduction over metal-organic framework-based materials. *Coord. Chem. Rev.* 2020, 412, 213262.
9. Liu, W.; Li, X.; Wang, C.; Pan, H.; Liu, W.; Wang, K.; Zeng, Q.; Wang, R.; Jiang, J. A scalable general synthetic approach toward ultrathin imine-linked two-dimensional covalent organic framework nanosheets for photocatalytic CO_2 reduction. *J. Am. Chem. Soc.* 2019, 141, 17431–17440.
10. Yang, C.; Huang, W.; da Silva, L.C.; Zhang, K.A.; Wang, X. Functional conjugated polymers for CO_2 reduction using visible light. *Chem. Eur. J.* 2018, 24, 17454–17458.
11. Yan, Y.; Chen, J.; Li, N.; Tian, J.; Li, K.; Jiang, J.; Liu, J.; Tian, Q.; Chen, P. Systematic bandgap engineering of graphene quantum dots and applications for photocatalytic water splitting and CO_2 reduction. *ACS Nano* 2018, 12, 3523–3532.
12. Sun, Z.; Wang, H.; Wu, Z.; Wang, L. g- C_3N_4 based composite photocatalysts for photocatalytic CO_2 reduction. *Catal. Today* 2018, 300, 160–172.

13. Gao, W.; Bai, X.; Gao, Y.; Liu, J.; He, H.; Yang, Y.; Han, Q.; Wang, X.; Wu, X.; Wang, J. Anchoring of black phosphorus quantum dots onto WO₃ nanowires to boost photocatalytic CO₂ conversion into solar fuels. *Chem. Comm.* 2020, 56, 7777–7780.
14. Ren, X.; Gao, M.; Zhang, Y.; Zhang, Z.; Cao, X.; Wang, B.; Wang, X. Photocatalytic reduction of CO₂ on BiOX: Effect of halogen element type and surface oxygen vacancy mediated mechanism. *Appl. Catal. B* 2020, 274, 119063.
15. Wang, H.; Zhang, L.; Wang, K.; Sun, X.; Wang, W. Enhanced photocatalytic CO₂ reduction to methane over WO₃·0.33 H₂O via Mo doping. *Appl. Catal. B* 2019, 243, 771–779.
16. Gao, M.; Yang, J.; Sun, T.; Zhang, Z.; Zhang, D.; Huang, H.; Lin, H.; Fang, Y.; Wang, X. Persian buttercup-like BiOBr_xCl_{1-x} solid solution for photocatalytic overall CO₂ reduction to CO and O₂. *Appl. Catal. B* 2019, 243, 734–740.
17. Samanta, S.; Yadav, R.; Kumar, A.; Sinha, A.K.; Srivastava, R. Surface modified C, O co-doped polymeric g-C₃N₄ as an efficient photocatalyst for visible light assisted CO₂ reduction and H₂O₂ production. *Appl. Catal. B* 2019, 259, 118054.
18. Shi, R.; Chen, Y. Controlled formation of defective shell on TiO₂ (001) facets for enhanced photocatalytic CO₂ reduction. *ChemCatChem* 2019, 11, 2270–2276.
19. Tu, W.; Zhou, Y.; Zou, Z. Photocatalytic conversion of CO₂ into renewable hydrocarbon fuels: State-of-the-art accomplishment, challenges, and prospects. *Adv. Mater.* 2014, 26, 4607–4626.
20. Razzaq, A.; In, S.-I. TiO₂ based nanostructures for photocatalytic CO₂ conversion to valuable chemicals. *Micromachines* 2019, 10, 326.
21. Huang, C.-Y.; Guo, R.-T.; Pan, W.-G.; Tang, J.-Y.; Zhou, W.-G.; Liu, X.-Y.; Qin, H.; Jia, P.-Y. One-dimension TiO₂ nanostructures with enhanced activity for CO₂ photocatalytic reduction. *Appl. Surf. Sci.* 2019, 464, 534–543.
22. Patil, S.B.; Basavarajappa, P.S.; Ganganagappa, N.; Jyothi, M.; Raghu, A.; Reddy, K.R. Recent advances in non-metals-doped TiO₂ nanostructured photocatalysts for visible-light driven hydrogen production, CO₂ reduction and air purification. *Int. J. Hydrog. Energy* 2019, 44, 13022–13039.
23. Xu, H.-M.; Wang, H.-C.; Shen, Y.; Lin, Y.-H.; Nan, C.-W. Low-dimensional nanostructured photocatalysts. *J. Adv. Ceram.* 2015, 4, 159–182.
24. Chang, X.; Wang, T.; Gong, J. CO₂ photo-reduction: Insights into CO₂ activation and reaction on surfaces of photocatalysts. *Energy Environ. Sci.* 2016, 9, 2177–2196.
25. Mao, J.; Li, K.; Peng, T. Recent advances in the photocatalytic CO₂ reduction over semiconductors. *Catal. Sci. Technol.* 2013, 3, 2481–2498.
26. Markovits, A.; Fahmi, A.; Minot, C. A theoretical study of CO₂ adsorption on TiO₂. *J. Mol. Struct. THEOCHEM* 1996, 371, 219–235.
27. Sharma, N.; Das, T.; Kumar, S.; Bhosale, R.; Kabir, M.; Ogale, S. Photocatalytic activation and reduction of CO₂ to CH₄ over single phase nano Cu₃SnS₄: A combined experimental and theoretical study. *ACS Appl. Energy Mater.* 2019, 2, 5677–5685.
28. Indrakanti, V.P.; Kubicki, J.D.; Schobert, H.H. Photoinduced activation of CO₂ on Ti-based heterogeneous catalysts: Current state, chemical physics-based insights and outlook. *Energy Environ. Sci.* 2009, 2, 745–758.
29. Álvarez, A.; Borges, M.; Corral-Pérez, J.J.; Olcina, J.G.; Hu, L.; Cornu, D.; Huang, R.; Stoian, D.; Urakawa, A. CO₂ activation over catalytic surfaces. *ChemPhysChem* 2017, 18, 3135–3141.
30. Fu, J.; Jiang, K.; Qiu, X.; Yu, J.; Liu, M. Product selectivity of photocatalytic CO₂ reduction reactions. *Mater. Today* 2020, 32, 222–243.
31. Khan, A.A.; Tahir, M. Recent advancements in engineering approach towards design of photo-reactors for selective photocatalytic CO₂ reduction to renewable fuels. *J. CO₂ Util.* 2019, 29, 205–239.
32. Linsebigler, A.L.; Lu, G.; Yates, J.T., Jr. Photocatalysis on TiO₂ surfaces: Principles, mechanisms, and selected results. *Chem. Rev.* 1995, 95, 735–758.
33. Hou, J.; Cao, S.; Wu, Y.; Gao, Z.; Liang, F.; Sun, Y.; Lin, Z.; Sun, L. Inorganic colloidal perovskite quantum dots for robust solar CO₂ reduction. *Chem. Eur. J.* 2017, 23, 9481–9485.
34. Sheng, J.; He, Y.; Li, J.; Yuan, C.; Huang, H.; Wang, S.; Sun, Y.; Wang, Z.; Dong, F. Identification of halogen-associated active sites on bismuth-based perovskite quantum dots for efficient and selective CO₂-to-CO photoreduction. *ACS Nano* 2020, 14, 13103–13114.
35. Zhou, L.; Xu, Y.F.; Chen, B.X.; Kuang, D.B.; Su, C.Y. Synthesis and Photocatalytic Application of Stable Lead-Free Cs₂AgBiBr₆ Perovskite Nanocrystals. *Small* 2018, 14, 1703762.

36. Que, M.; Zhao, Y.; Pan, L.; Yang, Y.; He, Z.; Yuan, H.; Chen, J.; Zhu, G. Colloidal formamidineum lead bromide quantum dots for photocatalytic CO₂ reduction. *Mater. Lett.* 2021, 282, 128695.
37. Zhu, C.; Wei, X.; Li, W.; Pu, Y.; Sun, J.; Tang, K.; Wan, H.; Ge, C.; Zou, W.; Dong, L. Crystal-Plane Effects of CeO₂ and CeO₂ on Photocatalytic CO₂ Reduction: Synergistic Interactions of Oxygen Defects and Hydroxyl Groups. *ACS Sustain. Chem. Eng.* 2020, 8, 14397–14406.
38. Liu, B.; Ye, L.; Wang, R.; Yang, J.; Zhang, Y.; Guan, R.; Tian, L.; Chen, X. Phosphorus-doped graphitic carbon nitride nanotubes with amino-rich surface for efficient CO₂ capture, enhanced photocatalytic activity, and product selectivity. *ACS Appl. Mater. Interfaces* 2018, 10, 4001–4009.
39. Mo, Z.; Zhu, X.; Jiang, Z.; Song, Y.; Liu, D.; Li, H.; Yang, X.; She, Y.; Lei, Y.; Yuan, S. Porous nitrogen-rich g-C₃N₄ nanotubes for efficient photocatalytic CO₂ reduction. *Appl. Catal. B* 2019, 256, 117854.
40. Di, J.; Zhu, C.; Ji, M.; Duan, M.; Long, R.; Yan, C.; Gu, K.; Xiong, J.; She, Y.; Xia, J. Defect-Rich Bi₁₂O₁₇Cl₂ Nanotubes Self-Accelerating Charge Separation for Boosting Photocatalytic CO₂ Reduction. *Angew. Chem. Int. Ed.* 2018, 57, 14847–14851.
41. Di, J.; Song, P.; Zhu, C.; Chen, C.; Xiong, J.; Duan, M.; Long, R.; Zhou, W.; Xu, M.; Kang, L. Strain-Engineering of Bi₁₂O₁₇Br₂ Nanotubes for Boosting Photocatalytic CO₂ Reduction. *ACS Mater. Lett.* 2020, 2, 1025–1032.
42. Xu, G.; Zhang, H.; Wei, J.; Zhang, H.-X.; Wu, X.; Li, Y.; Li, C.; Zhang, J.; Ye, J. Integrating the g-C₃N₄ Nanosheet with B–H bonding decorated metal–organic framework for CO₂ activation and photoreduction. *ACS Nano* 2018, 12, 5333–5340.
43. Xia, P.; Zhu, B.; Yu, J.; Cao, S.; Jaroniec, M. Ultra-thin nanosheet assemblies of graphitic carbon nitride for enhanced photocatalytic CO₂ reduction. *J. Mater. Chem. A* 2017, 5, 3230–3238.
44. Han, C.; Wang, B.; Wu, C.; Shen, S.; Zhang, X.; Sun, L.; Tian, Q.; Lei, Y.; Wang, Y. Ultrathin SiC nanosheets with high reduction potential for improved CH₄ generation from photocatalytic reduction of CO₂. *ChemistrySelect* 2019, 4, 2211–2217.
45. Di, J.; Zhao, X.; Lian, C.; Ji, M.; Xia, J.; Xiong, J.; Zhou, W.; Cao, X.; She, Y.; Liu, H. Atomically-thin Bi₂MoO₆ nanosheets with vacancy pairs for improved photocatalytic CO₂ reduction. *Nano Energy* 2019, 61, 54–59.
46. Dai, W.; Yu, J.; Luo, S.; Hu, X.; Yang, L.; Zhang, S.; Li, B.; Luo, X.; Zou, J. WS₂ quantum dots seeding in Bi₂S₃ nanotubes: A novel Vis-NIR light sensitive photocatalyst with low-resistance junction interface for CO₂ reduction. *Chem. Eng. J.* 2020, 389, 123430.
47. Zeng, Z.; Yan, Y.; Chen, J.; Zan, P.; Tian, Q.; Chen, P. Boosting the photocatalytic ability of Cu₂O nanowires for CO₂ conversion by MXene quantum dots. *Adv. Funct. Mater.* 2019, 29, 1806500.
48. Xie, Z.; Xu, Y.; Li, D.; Chen, L.; Meng, S.; Jiang, D.; Chen, M. Construction of CuO quantum Dots/WO₃ nanosheets 0D/2D Z-scheme heterojunction with enhanced photocatalytic CO₂ reduction activity under visible-light. *J. Alloys Compd.* 2021, 858, 157668.
49. Ong, W.-J.; Putri, L.K.; Tan, Y.-C.; Tan, L.-L.; Li, N.; Ng, Y.H.; Wen, X.; Chai, S.-P. Unravelling charge carrier dynamics in protonated g-C₃N₄ interfaced with carbon nanodots as co-catalysts toward enhanced photocatalytic CO₂ reduction: A combined experimental and first-principles DFT study. *Nano Res.* 2017, 10, 1673–1696.
50. Shi, H.; Long, S.; Hu, S.; Hou, J.; Ni, W.; Song, C.; Li, K.; Gurzadyan, G.G.; Guo, X. Interfacial charge transfer in 0D/2D defect-rich heterostructures for efficient solar-driven CO₂ reduction. *Appl. Catal. B* 2019, 245, 760–769.
51. Wang, R.; Shen, J.; Sun, K.; Tang, H.; Liu, Q. Enhancement in photocatalytic activity of CO₂ reduction to CH₄ by 0D/2D Au/TiO₂ plasmon heterojunction. *Appl. Surf. Sci.* 2019, 493, 1142–1149.
52. Wang, J.; Wang, J.; Li, N.; Du, X.; Ma, J.; He, C.; Li, Z. Direct Z-Scheme 0D/2D Heterojunction of CsPbBr₃ Quantum Dots/Bi₂WO₆ Nanosheets for Efficient Photocatalytic CO₂ Reduction. *ACS Appl. Mater. Interfaces* 2020, 12, 31477–31485.
53. Xu, F.; Zhu, B.; Cheng, B.; Yu, J.; Xu, J. 1D/2D TiO₂/MoS₂ hybrid nanostructures for enhanced photocatalytic CO₂ reduction. *Adv. Opt. Mater.* 2018, 6, 1800911.
54. Tahir, M.; Tahir, B.; Nawawi, M.; Hussain, M.; Muhammad, A. Cu-NPs embedded 1D/2D CNTs/pCN heterojunction composite towards enhanced and continuous photocatalytic CO₂ reduction to fuels. *Appl. Surf. Sci.* 2019, 485, 450–461.
55. Bian, J.; Qu, Y.; Zhang, X.; Sun, N.; Tang, D.; Jing, L. Dimension-matched plasmonic Au/TiO₂/BiVO₄ nanocomposites as efficient wide-visible-light photocatalysts to convert CO₂ and mechanistic insights. *J. Mater. Chem. A* 2018, 6, 11838–11845.

56. Cao, S.; Shen, B.; Tong, T.; Fu, J.; Yu, J. 2D/2D heterojunction of ultrathin MXene/Bi₂WO₆ nanosheets for improved photocatalytic CO₂ reduction. *Adv. Funct. Mater.* 2018, 28, 1800136.
57. Kong, X.Y.; Lee, W.Q.; Mohamed, A.R.; Chai, S.-P. Effective steering of charge flow through synergistic inducing oxygen vacancy defects and pn heterojunctions in 2D/2D surface-engineered Bi₂WO₆/BiOI cascade: Towards superior photocatalytic CO₂ reduction activity. *Chem. Eng. J.* 2019, 372, 1183–1193.
58. Tahir, B.; Tahir, M.; Yunus, M.A.C.; Mohamed, A.R.; Siraj, M.; Fatehmulla, A. 2D/2D Mt/m-CN composite with enriched interface charge transfer for boosting photocatalytic CO₂ hydrogenation by H₂ to CH₄ under visible light. *Appl. Surf. Sci.* 2020, 520, 146296.
59. She, H.; Zhou, H.; Li, L.; Zhao, Z.; Jiang, M.; Huang, J.; Wang, L.; Wang, Q. Construction of a two-dimensional composite derived from TiO₂ and SnS₂ for enhanced photocatalytic reduction of CO₂ into CH₄. *ACS Sustain. Chem. Eng.* 2018, 7, 650–659.
60. Lu, M.; Li, Q.; Zhang, C.; Fan, X.; Li, L.; Dong, Y.; Chen, G.; Shi, H. Remarkable photocatalytic activity enhancement of CO₂ conversion over 2D/2D g-C₃N₄/BiVO₄ Z-scheme heterojunction promoted by efficient interfacial charge transfer. *Carbon* 2020, 160, 342–352.
61. Huo, Y.; Zhang, J.; Wang, Z.; Dai, K.; Pan, C.; Liang, C. Efficient interfacial charge transfer of 2D/2D porous carbon nitride/bismuth oxychloride step-scheme heterojunction for boosted solar-driven CO₂ reduction. *J. Colloid Interface Sci.* 2021, 585, 684–693.
62. Zhang, R.; Huang, Z.; Li, C.; Zuo, Y.; Zhou, Y. Monolithic g-C₃N₄/reduced graphene oxide aerogel with in situ embedding of Pd nanoparticles for hydrogenation of CO₂ to CH₄. *Appl. Surf. Sci.* 2019, 475, 953–960.
63. Akhundi, A.; Habibi-Yangjeh, A.; Abitorabi, M.; Rahim Pouran, S. Review on photocatalytic conversion of carbon dioxide to value-added compounds and renewable fuels by graphitic carbon nitride-based photocatalysts. *Catal. Rev.* 2019, 61, 595–628.
64. He, Z.; Zhang, J.; Li, X.; Guan, S.; Dai, M.; Wang, S. 1D/2D Heterostructured Photocatalysts: From Design and Unique Properties to Their Environmental Applications. *Small* 2020, 16, 2005051.
65. Li, B.; Cao, Z.; Wang, S.; Wei, Q.; Shen, Z. BiVO₄ quantum dot-decorated BiPO₄ nanorods 0D/1D heterojunction for enhanced visible-light-driven photocatalysis. *Dalton Trans.* 2018, 47, 10288–10298.
66. Jo, W.-K.; Kumar, S.; Eslava, S.; Tonda, S. Construction of Bi₂WO₆/RGO/g-C₃N₄ 2D/2D/2D hybrid Z-scheme heterojunctions with large interfacial contact area for efficient charge separation and high-performance photoreduction of CO₂ and H₂O into solar fuels. *Appl. Catal. B* 2018, 239, 586–598.
67. He, F.; Zhu, B.; Cheng, B.; Yu, J.; Ho, W.; Macyk, W. 2D/2D/0D TiO₂/C₃N₄/Ti₃C₂ MXene composite S-scheme photocatalyst with enhanced CO₂ reduction activity. *Appl. Catal. B* 2020, 272, 119006.
68. Fu, J.; Zhu, B.; Jiang, C.; Cheng, B.; You, W.; Yu, J. Hierarchical porous O-doped g-C₃N₄ with enhanced photocatalytic CO₂ reduction activity. *Small* 2017, 13, 1603938.
69. Gao, J.; Shen, Q.; Guan, R.; Xue, J.; Liu, X.; Jia, H.; Li, Q.; Wu, Y. Oxygen vacancy self-doped black TiO₂ nanotube arrays by aluminothermic reduction for photocatalytic CO₂ reduction under visible light illumination. *J. CO₂ Util.* 2020, 35, 205–215.
70. Xiu, Z.; Guo, M.; Zhao, T.; Pan, K.; Xing, Z.; Li, Z.; Zhou, W. Recent advances in Ti³⁺ self-doped nanostructured TiO₂ visible light photocatalysts for environmental and energy applications. *Chem. Eng. J.* 2020, 382, 123011.
71. Wang, H.; Liu, X.; Niu, P.; Wang, S.; Shi, J.; Li, L. Porous two-dimensional materials for photocatalytic and electrocatalytic applications. *Matter* 2020, 2, 1377–1413.
72. Tian, N.; Xiao, K.; Zhang, Y.; Lu, X.; Ye, L.; Gao, P.; Ma, T.; Huang, H. Reactive sites rich porous tubular yolk-shell g-C₃N₄ via precursor recrystallization mediated microstructure engineering for photoreduction. *Appl. Catal. B* 2019, 253, 196–205.